

The interplay of intersystem crossing and internal conversion in quadrupolar tetraarylpyrrolo[3,2-b]pyrroles

Krzysztof Górska,^a Damian Kusy,^a Shuhei Ozaki,^{b,c} Marzena Banasiewicz,^d Rashid Valiev,^e Smruti Ranjan Sahoo,^f Kenji Kamada,^{*b,c} Glib Baryshnikov,^{*f} Daniel T. Gryko^{*a}

^a Institute of Organic Chemistry, Polish Academy of Sciences, Kasprzaka 44/52, 01-224 Warsaw, Poland. E-mail: dtgryko@icho.edu.pl.

^b NMRI, National Institute of Advanced Industrial Science and Technology (AIST), Ikeda, Osaka 563-8577, Japan.

^c Department of Chemistry, Graduate School of Science and Technology, Kwansei Gakuin University, Sanda 669-1337, Japan.

^d Institute of Physics, Polish Academy of Sciences, Al. Lotników 32/46, 02-668 Warsaw, Poland.

^e Department of Chemistry, University of Helsinki, FI-00014 Helsinki, Finland

^f Laboratory of Organic Electronics, Department of Science and Technology, Linköping University, SE-60174 Norrköping, Sweden

Table of Content

1. Synthesis, analytical and spectral data	1
2. Two-photon absorption measurement.....	8
3. Computational Methodology	12
4. References.....	17

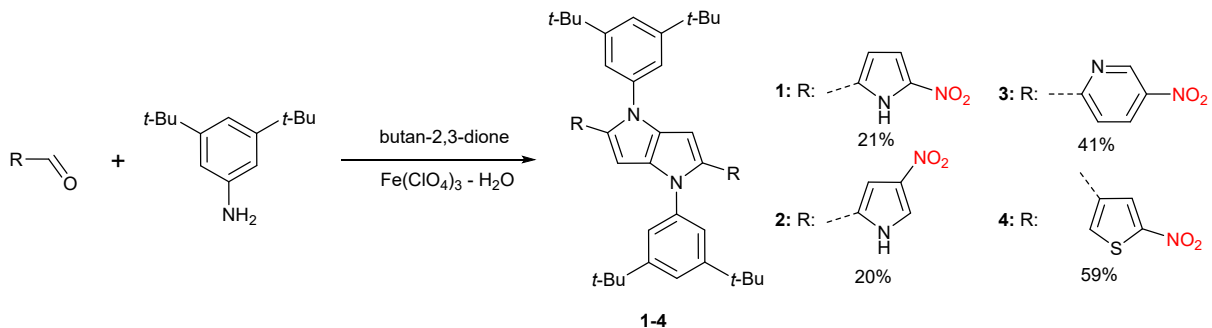
1. Synthesis, analytical and spectral data

Experimental:

All chemicals were used as received unless otherwise noted. All used for reaction solvents were pure for analysis grade and were taken without further purification. **4-Nitro-1H-pyrrole-2-carboxaldehyde** and **5-Nitro-1H-pyrrole-2-carboxaldehyde** was synthesized according to literature procedure^[1] while **5-Nitro-3-thiophenecarboxaldehyde** was bought from Apollo Scientific, **5-Nitropicolinaldehyde** from Aldrich and **3,5-di-t-butylaniline** from TCI. All reactions requiring heating were carried out using an oil bath. All reported NMR spectra were recorded on a 500 MHz spectrometer. Chemical shifts (δ ppm) for ^1H and $^{13}\text{C}\{^1\text{H}\}$ NMR were determined to solvent residual signal as the internal reference; J values are given in Hz. UV/Vis absorption spectra were recorded on a PerkinElmer Lambda 35 Spectrometer. Fluorescence spectra were recorded on a FLS1000 of Edinburgh Instruments. Absorption spectra were recorded in n-hexane, toluene, propyl butyrate, tetrahydrofuran, ethyl acetate n-octanol, n-butyl acetate, acetonitrile and methanol. In order to determine the fluorescence quantum yield Rh6G in EtOH, Rh101 in MeOH and Coum153 in EtOH were used as a quantum yield standard. Chromatography was performed on silica (Kieselgel 60, 200-400 mesh). Mass spectra were obtained with EI ion source and the EBE double-focusing geometry mass analyzer or spectrometer equipped with electrospray ion source with q-TOF type mass analyzer.

General procedure for the synthesis of 1,4-dihydro-pyrrolo[3,2-b]pyrroles:^[2]

In an open round-bottom flask, aldehyde (8mmol) and 3,5-di-t-butylaniline (8mmol) were dissolved in a mixture of 6ml of toluene and 6ml of acetic acid. The obtained yellow solution was heated up to 50°C (precipitate may appear). After 1h in constant temperature butane-1,2-dione (4mmol) and catalytic amount of iron(III) chlorate(VII) monohydrate (3%mol) were added. The mixture turns dark and after a while precipitate appears. After 24 hours of stirring at 50 °C under open air, the solution was cooled and the formed precipitate was filtered off.



Scheme S1: Synthesis of 1,4-dihydro-pyrrolo[3,2-b]pyrroles and reaction yields

1 was obtained as grey-brown solid, yield 551mg (20%). ¹H NMR (500 MHz, d6-acetone) δ: 11.53 (s, 2H), 7.55 (t, J = 1.7 Hz, 2H), 7.28 (d, J = 1.7 Hz, 4H), 7.02 (d, J = 4.3 Hz, 2H), 6.82 (s, 2H), 5.74 (d, J = 4.2 Hz, 2H), 1.34 (s, 36H). ¹³C {¹H} NMR (126 MHz, d6-acetone) δ: 152.3, 138.4, 132.8, 131.3, 127.4, 120.9, 120.0, 112.0, 110.1, 94.7, 34.7, 30.7. HRMS (EI): m/z calculated for C₄₂H₅₀N₆O₄: 702.3894 [M⁺]; found: 702.3899.

2 was obtained as brick-red solid, yield 579mg (21%). ¹H NMR (500 MHz, d6-acetone) δ: 11.07 (s, 1H), 7.77 (dd, J = 3.4, 1.7 Hz, 2H), 7.52 (t, J = 1.7 Hz, 2H), 7.28 (d, J = 1.7 Hz, 4H), 6.55 (s, 2H), 6.23 (dd, J = 2.7, 1.8 Hz, 2H), 1.34 (s, 36H). ¹³C {¹H} NMR (126 MHz, d6-acetone) δ: 152.0, 138.5, 137.5, 131.0, 126.6, 126.2, 120.4, 119.8, 119.5, 102.4, 93.6, 34.7, 30.7. HRMS (EI): m/z calculated for C₄₂H₅₀N₆O₄: 702.3894 [M⁺]; found: 702.3897.

3 was obtained as red solid, yield 290 mg (41%) ¹H NMR (500 MHz, Chloroform-*d*) δ 9.31 (d, *J* = 2.6 Hz, 2H), 8.15 (dd, *J* = 9.0, 2.6 Hz, 2H), 7.43 (s, 2H), 7.16 (s, 4H), 6.99 (s, 2H), 6.93 (d, *J* = 9.0 Hz, 2H), 1.31 (s, 36H), ¹³C NMR (126 MHz, Chloroform-*d*) δ 156.2, 152.9, 145.5, 141.0, 138.7, 137.2, 136.2, 130.6, 121.2, 120.7, 120.4, 99.3, 35.2, 31.5. HRMS (EI): m/z calculated for C₄₄H₅₀N₆O₄: 726.3894 [M⁺]; found: 726.3883.

4 was obtained as orange solid, yield 1.73g (59%). ¹H NMR (500 MHz, CD₂Cl₂) δ: 7.73 (d, *J* = 1.7 Hz, 2H), 7.46 (s, 2H), 7.18 (d, *J* = 1.4 Hz, 4H), 6.99 (d, *J* = 1.7 Hz, 2H), 6.42 (s, 2H), 1.33 (s, 36H). ¹³C {¹H} NMR (126 MHz, CD₂Cl₂) δ: 153.0, 151.7, 138.5, 134.5, 131.8, 130.1, 128.7, 126.8, 121.2, 120.4, 94.3, 35.3, 31.4. HRMS (EI): m/z calculated for C₄₂H₄₈N₂O₄S₂: 736.3117 [M⁺]; found: 736.3123.

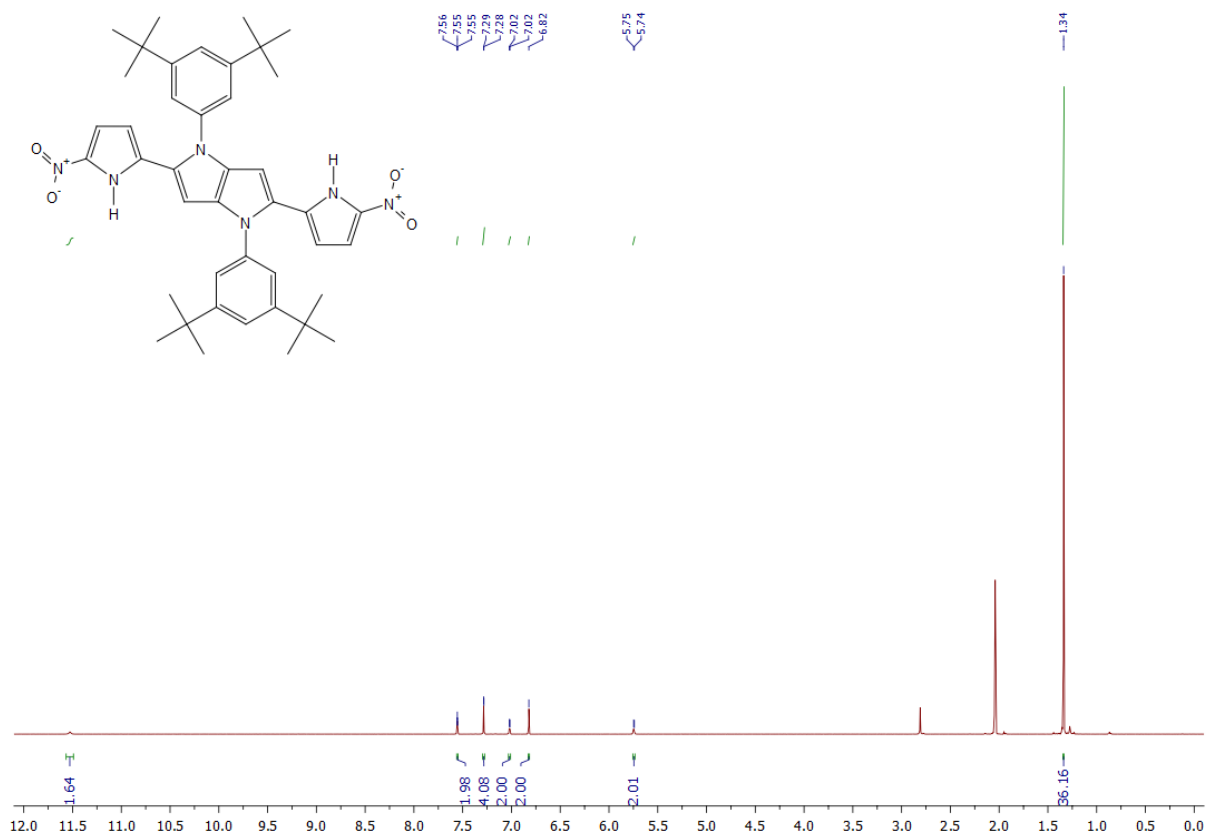


Fig. S1: 500 MHz ^1H NMR spectrum of 1 in d_6 -acetone

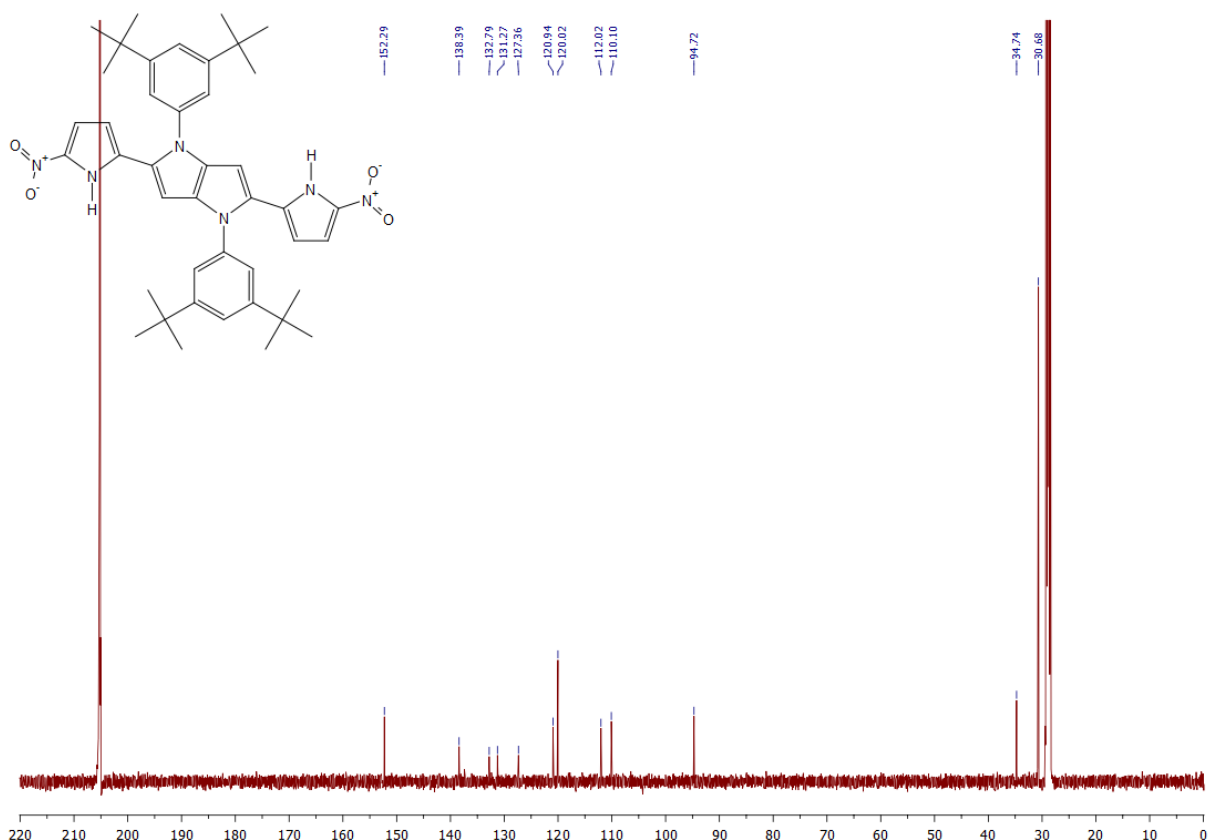


Fig. S2: 126 MHz ^{13}C { ^1H } NMR spectrum of 1 in d_6 -acetone

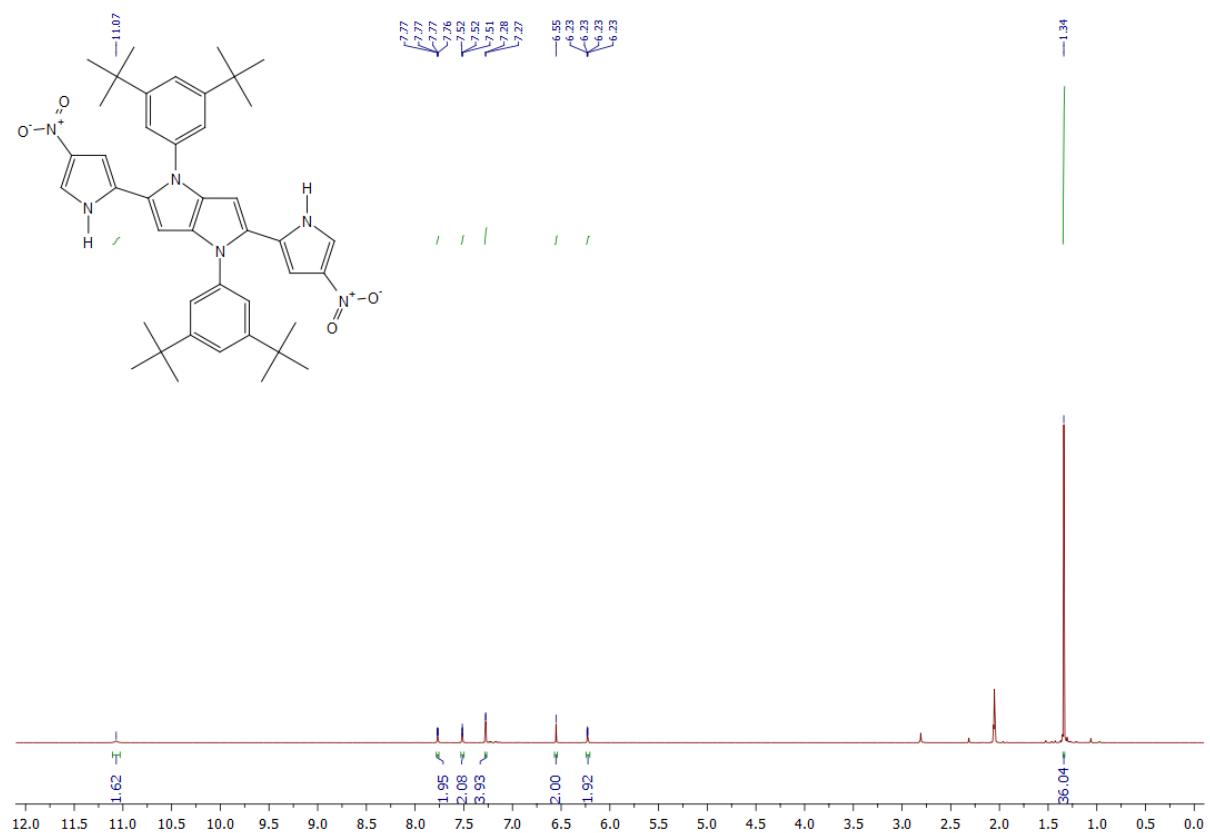


Fig. S3: 500 MHz ^1H NMR spectrum of 2 in d_6 -acetone

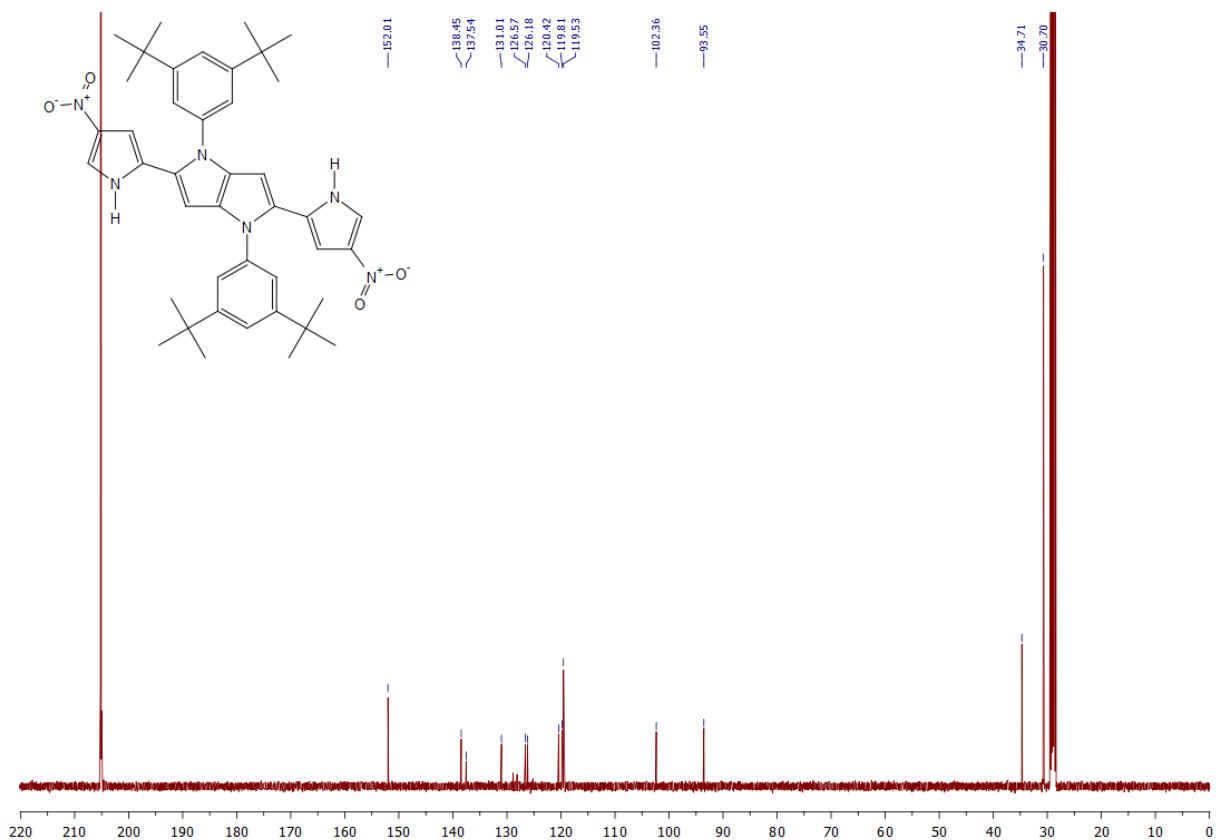


Fig. S4: 126 MHz ^{13}C { ^1H } NMR spectrum of 2 in d_6 -acetone

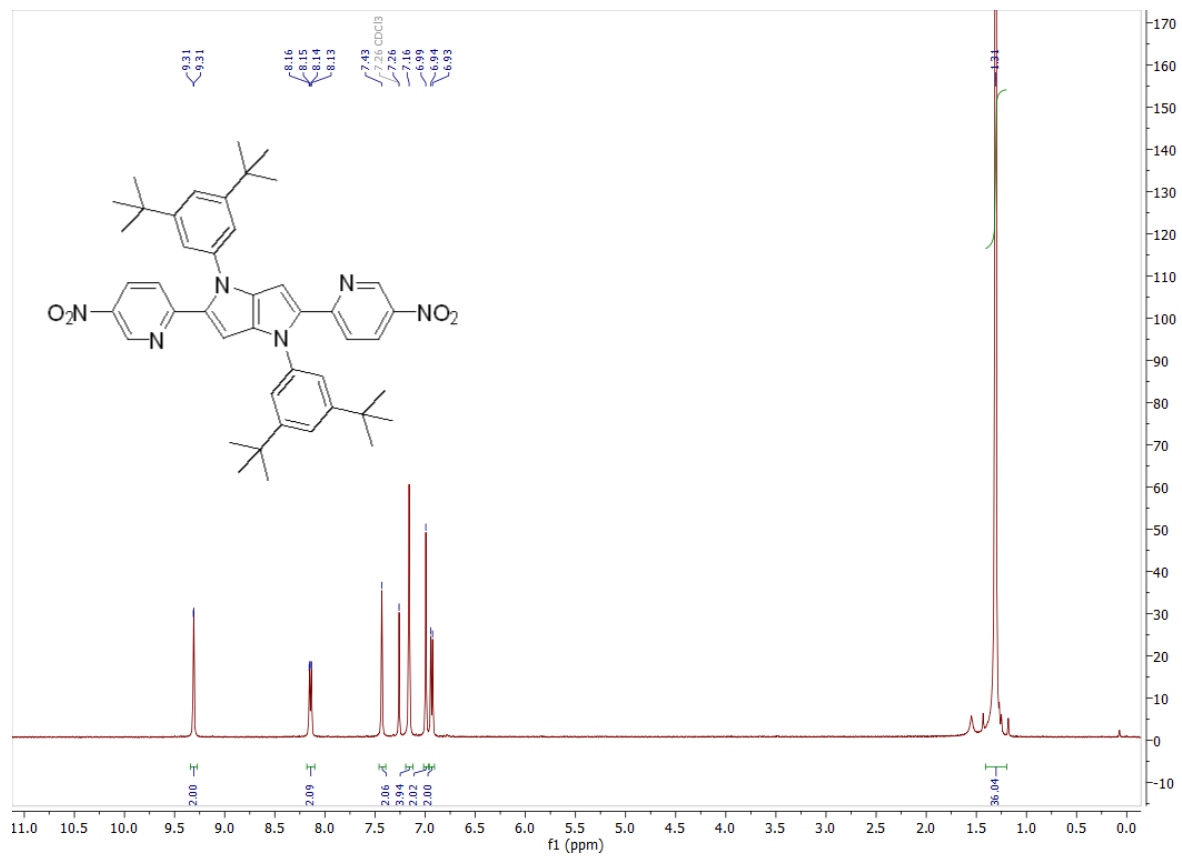


Fig. S5: 500 MHz ^1H NMR spectrum of 3 in CDCl_3

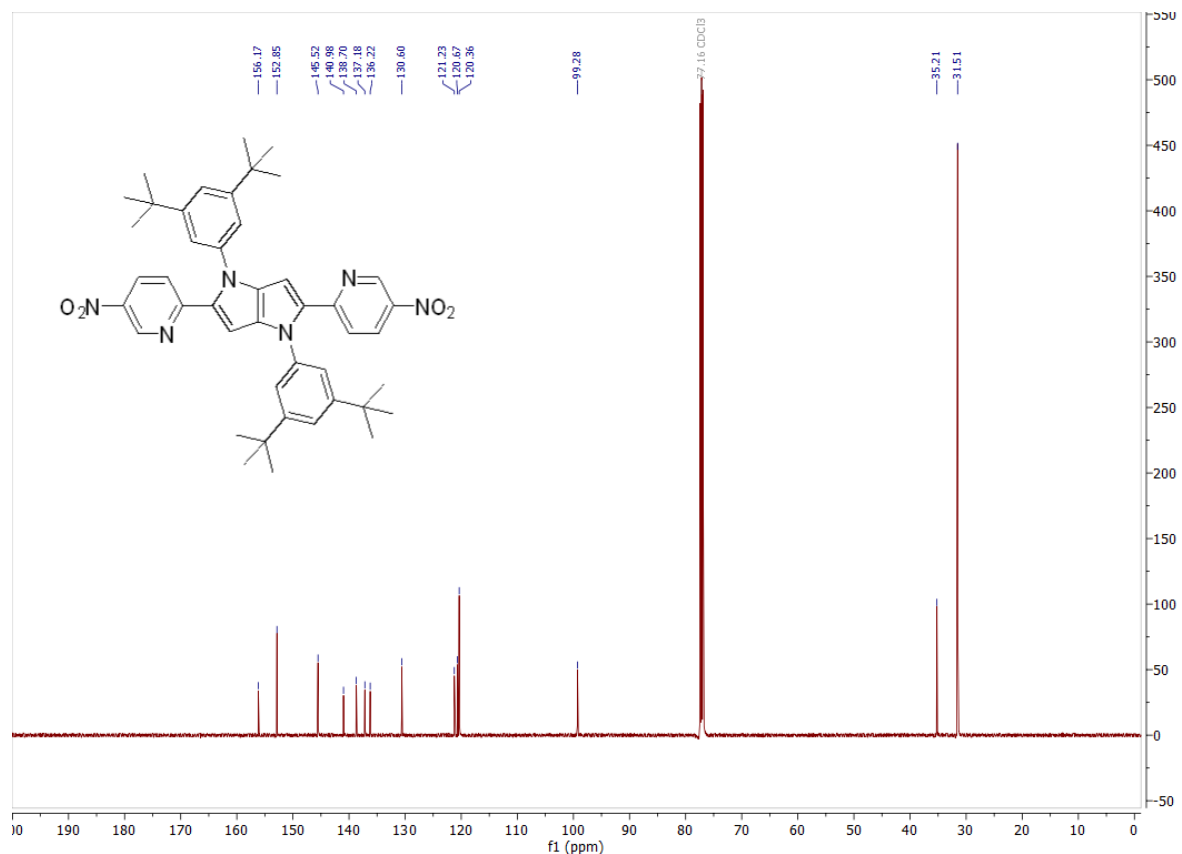


Fig. S6: 126 MHz $^{13}\text{C}\{^1\text{H}\}$ NMR spectrum of 3 in CDCl_3

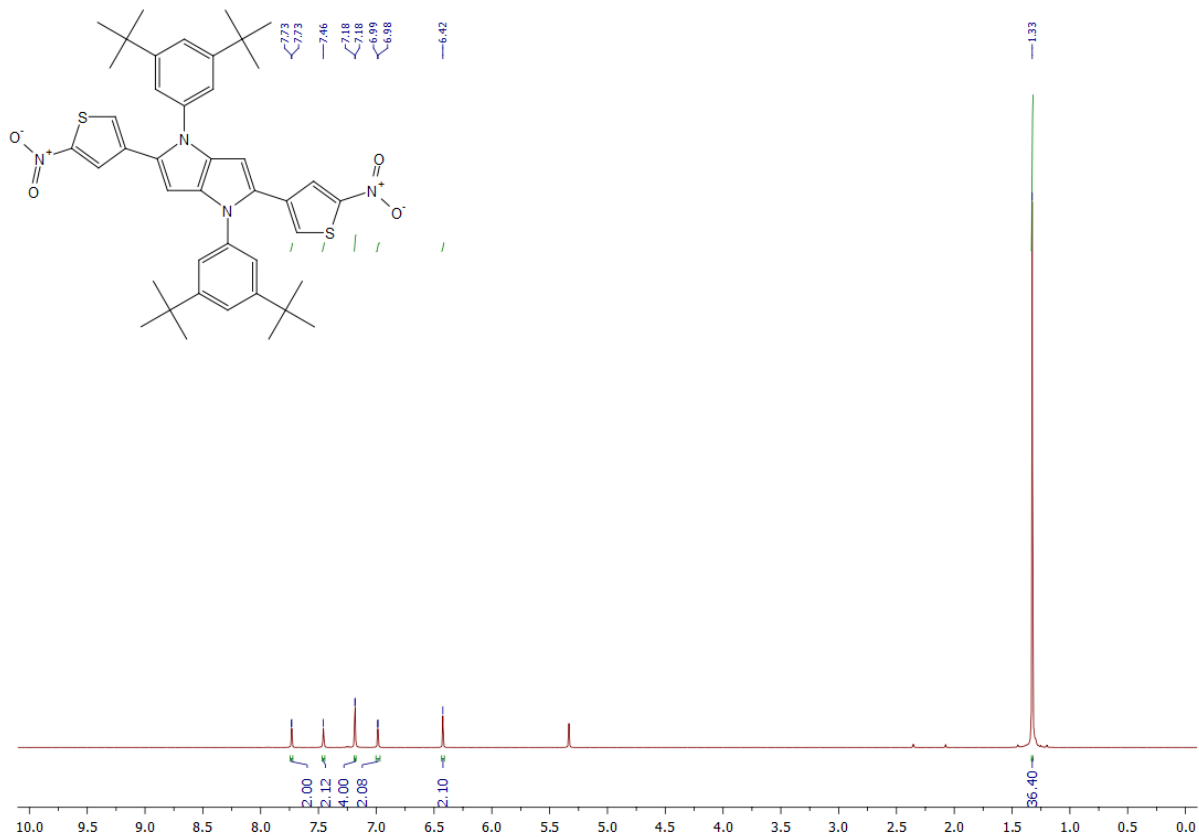


Fig. S7: 500 MHz ^1H NMR spectrum of 4 in CD_2Cl_2

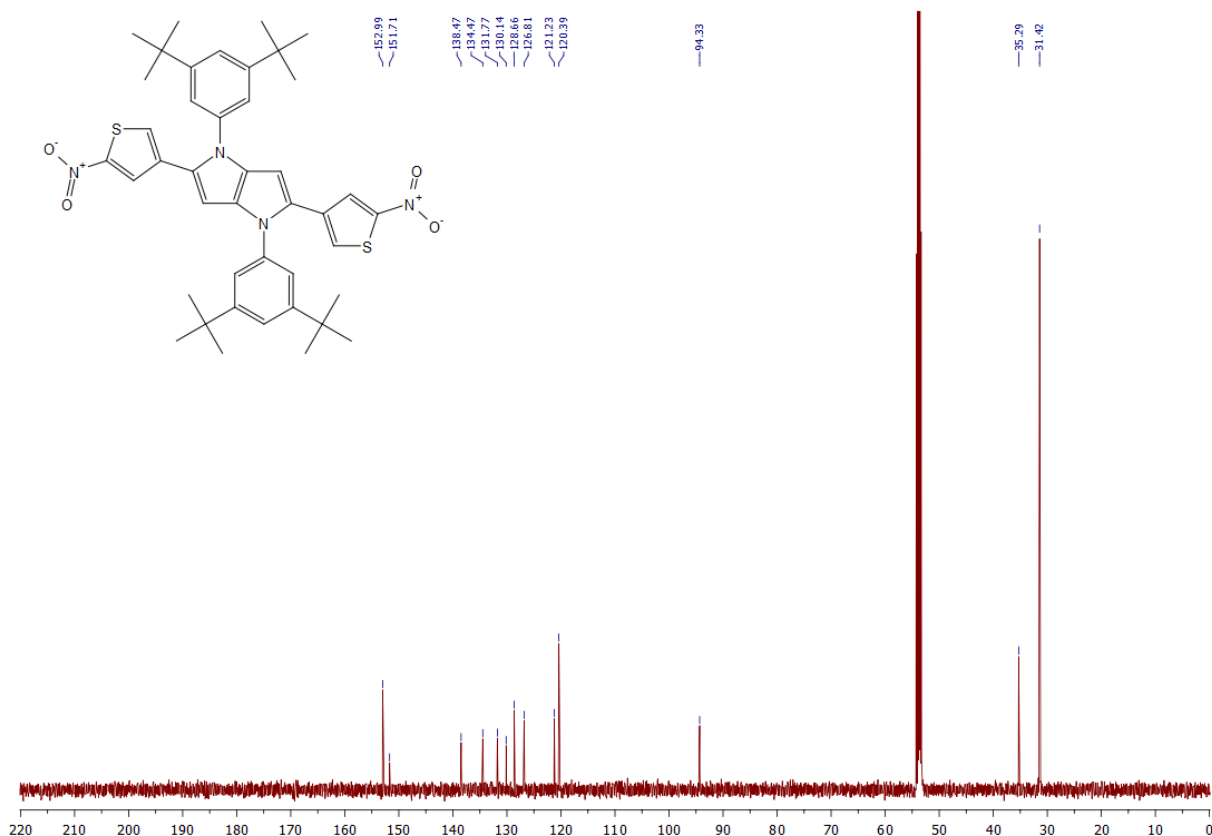


Fig. S8: 126 MHz ^{13}C { ^1H } NMR spectrum of 4 in CD_2Cl_2

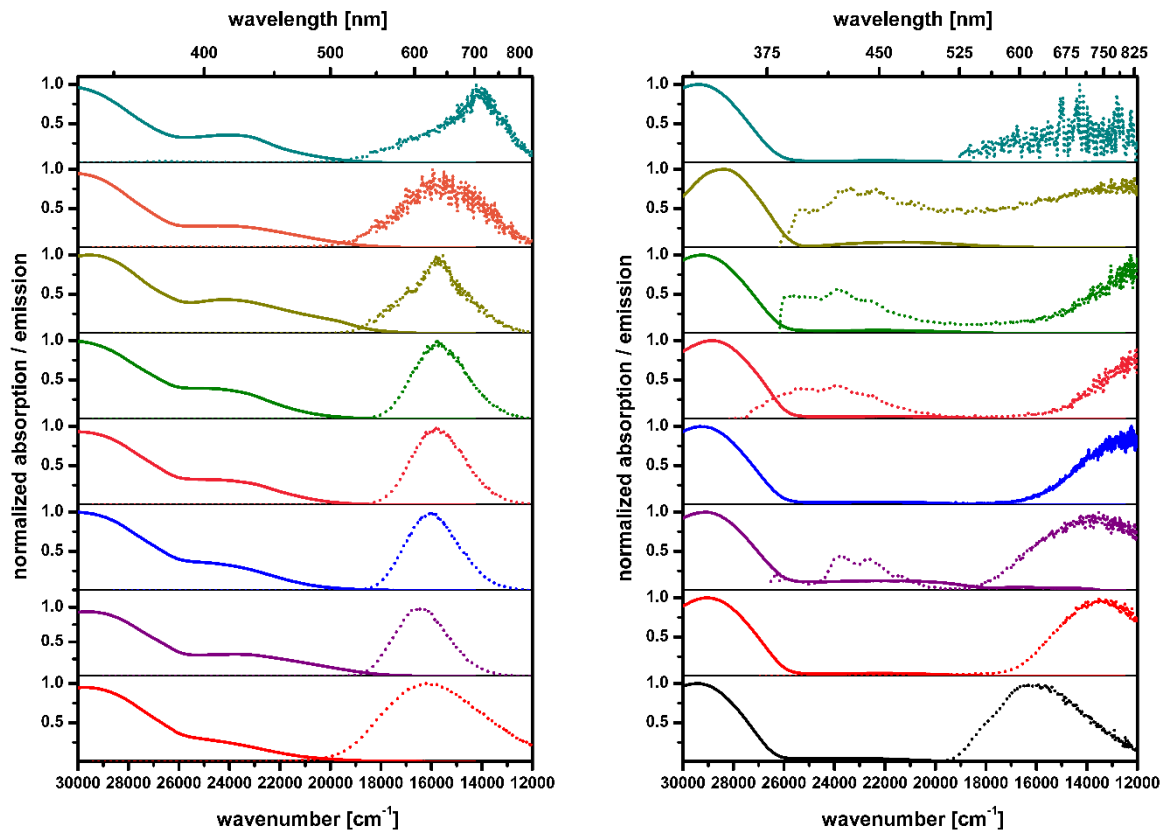


Fig. S9: Absorption (solid) and emission (dot) spectra of **2** (left) and **4** (right) in hexane (black), toluene (red), n-octanol (purple), propyl butyrate (blue), tetrahydrofuran (pink), ethyl acetate (green), butyl acetate (gold), acetonitrile (cyan)

2. Two-photon absorption measurement

The open-aperture Z-scan method^[3] was employed for two-photon absorption (TPA) spectrum measurements. A femtosecond optical parametric amplifier (Spectra-Physics TOPAS Prime) was used as wavelength-tunable light source. The setup was reported previously in detail.^[4] Open-aperture Z-scan trace acquired was analyzed by the curve fitting with the following equation,

$$T(\zeta) = T_N \frac{1}{\sqrt{\pi} q(\zeta)} \int_{-\infty}^{+\infty} \ln[1 + q(\zeta) e^{-x^2}] dx \quad \#(E1)$$

Here $T(\zeta)$ is the transmittance of the sample as function of normalized sample position $\zeta = z/z_R$ with the Rayleigh length z_R for a two-photon absorber excited by spatially and temporally Gaussian pulses. $T_N = \exp(-\alpha L)$ is linear transmittance of the sample, α is linear absorption coefficient, and L is physical path length of the sample. $q(\zeta)$ is on-axis two-photon absorbance $q(\zeta) = q_0/(1 + \zeta^2)$ with the on-axis two-photon absorbance at the sample position $q(0) = q_0$. This q_0 is related with two-photon absorption coefficient β as,

$$q_0 = \beta I_0 L \quad \#(E2)$$

where I_0 is the on-axis peak intensity of the incident Gaussian pulse. For the measurement performed by using a fixed incident power (i.e., a fixed I_0), β was calculated by assuming the proportionality relation of eq. S2. We call the measurement mode with a fixed incident power and repeating the measurement by changing the wavelength as “Wavelength(WL) Scan”, which results in high throughput of the spectral measurement. However, the assumption that the no other mechanism rather than TPA contributes to the signal does not hold always. For example, excited state absorption (ESA) or three-photon absorption may also contribute to the signal (transmittance dip around the focal point). So, we also recorded the incident-power dependence (i.e., by changing I_0) at some wavelengths to check the proportionality shown by eq. S2. We call the second measurement mode is “Power Scan”. In this case, β was determined from the slope of the plot of q_0 against I_0 .

Finally, TPA cross section $\sigma^{(2)}$ was obtained from β by using the convention $\sigma^{(2)} = hv\beta/N$, where hv is photon energy of excitation pulse and N is number density of sample molecule calculated from the concentration. The unit of Göppert-Mayer (GM) was used for TPA cross section where $1 \text{ GM} = 10^{-50} \text{ cm}^4 \text{ s photon}^{-1} \text{ molecule}^{-1}$.

For all compounds, 1–2 mM solution in spectroscopic grade chloroform (Fuji Film-Wako) hold in 2-mm quartz cuvette was used for Z-scan measurement. The path length is short enough against z_R (9–11 mm) to satisfy the thin sample condition^[3] for eq. S1. The sample solution was stirred during the measurement by a micro rotor put in the cell to avoid unwanted effect by the sample bleaching and photoproduct. No significant degradation was observed for both samples after Z-scan measurements, which is confirmed by UV-vis measurements. For calibration of day-by-day fluctuation of the measured values, inhouse standard materials were measured at the same time with the samples (MPPBT in dimethyl sulfoxide^[5]).

At short wavelengths where the tail of linear absorption (one-photon absorption, OPA) exists, saturable absorption (SA) of OPA was overlaps on open-aperture Z-scan trace. For such cases, the traces were analyzed with eq. S1 by replacing α with phenomenological modeling of SA as

$$\alpha \Rightarrow \alpha(I(\zeta)) = \frac{\alpha_0}{(1 + I(\zeta)/I_s)} \quad \#(E3)$$

where I_s is saturation intensity and $I(\zeta) = I_0/(1 + \zeta^2)$.^[6]

Some examples of the acquired open-aperture Z-scan traces at typical wavelengths are shown in Figs. S10–S13. Example of the SA+TPA signal was shown in Fig. S14.

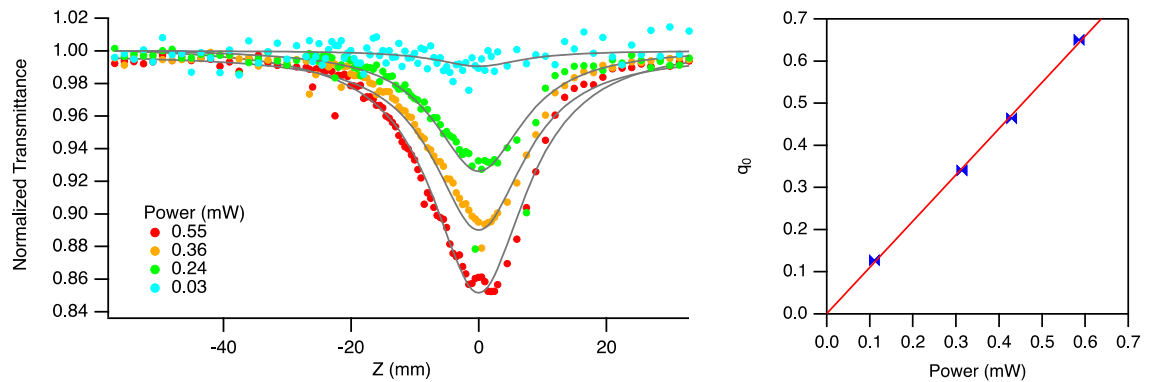


Fig. S10: (left) Open-aperture Z-scan traces of **1** in chloroform (2.0 mM) measured at 900 nm at different incident powers (symbols) with theoretical fits with eq. E1 (grey curves). (right) The corresponding plot of the two-photon absorbance q_0 obtained from the curve fits against the incident power in the left panel.

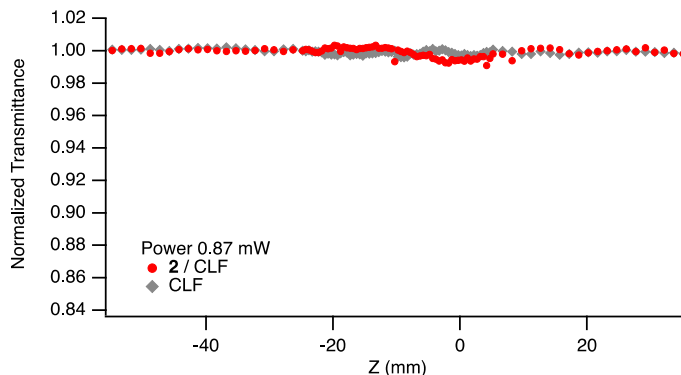


Fig. S11: (left) Open-aperture Z-scan traces of **2** in chloroform (1.4 mM) measured at 800 nm (red circle) and neat solvent (grey diamond) as control.

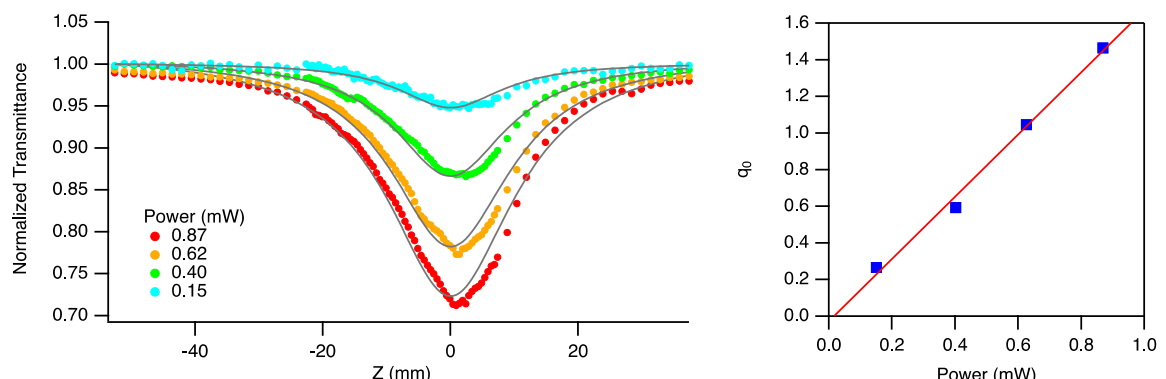


Fig. S12: (left) Open-aperture Z-scan traces of **3** in chloroform (0.93 mM) measured at 800 nm at different incident powers (symbols) with theoretical fits with eq. E1 (grey curves). (right) The corresponding plot of the two-photon absorbance q_0 obtained from the curve fits against the incident power in the left panel.

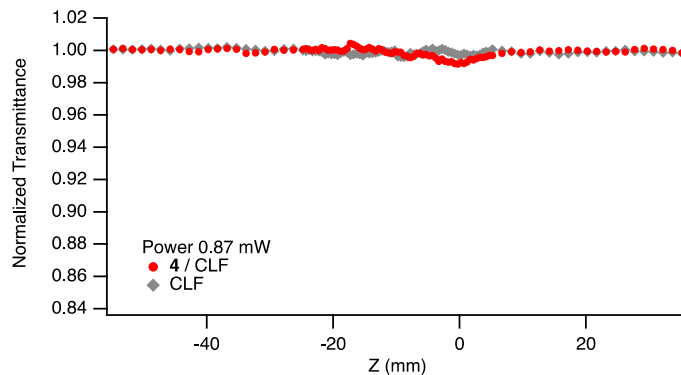


Fig. S13: (left) Open-aperture Z-scan traces of **2** in chloroform (1.9 mM) measured at 800 nm (red circle) and neat solvent (gray diamond) as control.

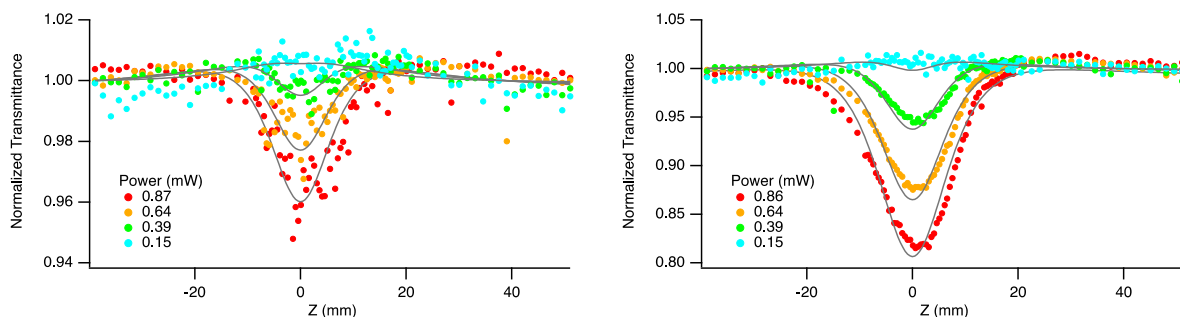


Fig. S14: Example of the open-aperture Z-scan traces affected by saturable absorption of one-photon absorption. (left) **2** in chloroform (1.3 mM) and (right) **3** in chloroform (2.1 mM) both measured at 600 nm at different incident powers (symbols) with theoretical fits with eq. E1 with eq. E3.

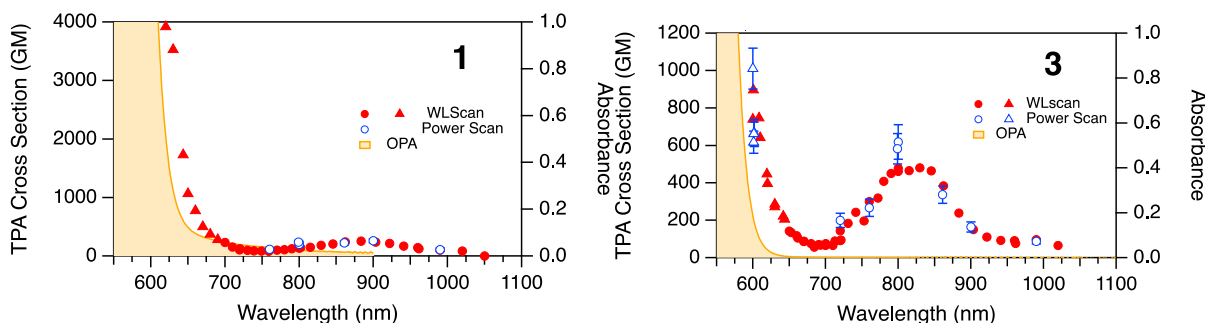
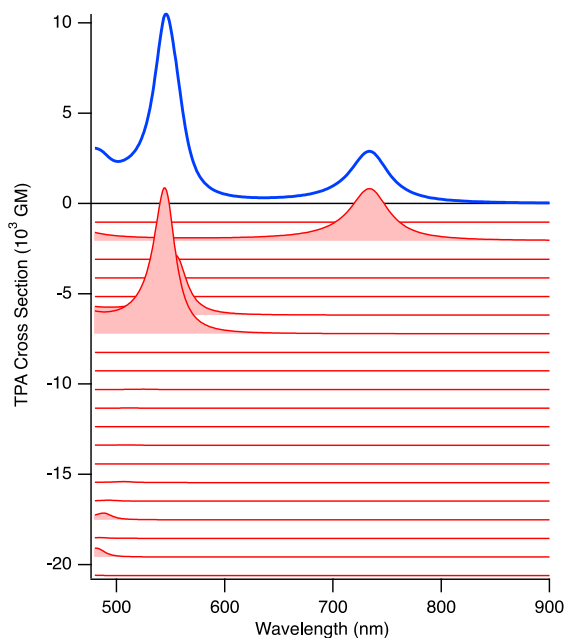
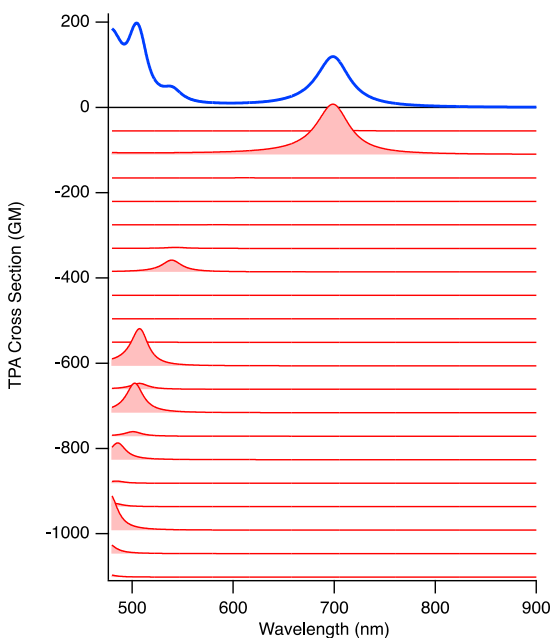


Fig. S15: Two-photon absorption spectra of the quadrupolar dyes **1** and **3** (circles and triangles) in chloroform to bottom and left axes. The data points out of vertical range in Fig. 3 in the main text are also shown here. The data shown with triangle were affected by the saturable absorption (SA) and analysed by considering it. The filled symbols are the data measured with a single incident power (WL-scan), and the open symbols with error bars are those measured by varying the incident power (power scan). See Experimental for the details on the modes of measurements and the analysis of the mixed data of TPA and SA. The one-photon absorption (OPA) spectra (to right and bottom axes) of the same solutions in the same cells used for the Z-scan measurements are also shown with the area filled with pale orange.

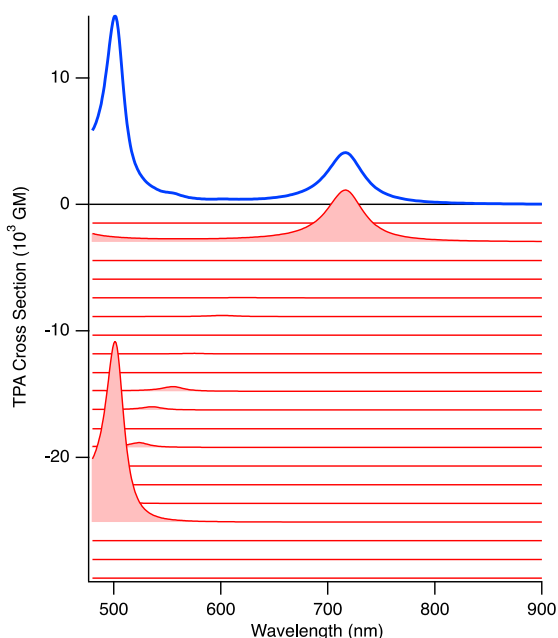
1



2



3



4

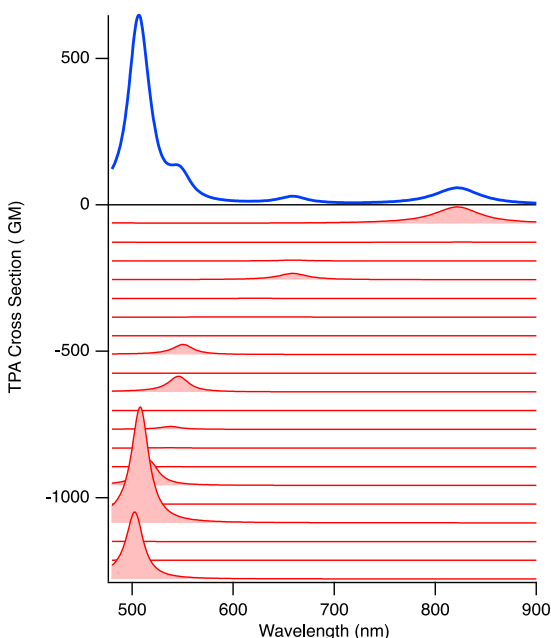


Fig. S16: Simulated two-photon absorption spectra (blue curve) of the quadrupolar dyes **1–4**. The geometry optimization and the property (transition energy and transition dipole moment) calculations were performed at the CAM-B3LYP/6-31+G(d). Up to 20 excited singlet states were considered. Solvent effect was considered by using the PCM model (chloroform). The red curves are the decomposed spectra by the final state ($S_0 \rightarrow S_n$), from top to bottom, $n=1, 2, \dots, 20$.

The CAM-B3LYP/6-31+G(d) level of theory was used for geometry optimization of molecular structure. Solvent effect was considered by applying polarizable continuum model (PCM) for chloroform. Transition dipole moments and transition energies, and permanent dipole moments were calculated for the lowest 20 excited state by using the Tamm-Dancoff Approximation (TDA)^[7] with the same level of theory (CAM-B3LYP/6-31+G(d)). Gaussian16 program suit^{[8],[9]} was used for all calculations. For TPA spectrum simulation, we used homemade program running on Igor Pro (Wavemetrics Inc.) based on the reported equations.^[10]

3. Computational Methodology

We used density functional theory (DFT) level with B3LYP hybrid functional and 6-31G(d,p) basis for the ground state (S_0) molecular optimization of dyes **1 – 4**. The Grimme's GD3 version dispersion function was included to the hybrid function during the optimization. With the dispersion included optimized S_0 geometries in hand, we performed singlet excitation up to five excited states and lowest singlet excited state (S_1) geometry relaxation as well using the time-dependent density functional theory (TDDFT) with the hybridization of exchange-correlation functional BLYP with the 37% of Hartree-Fock (HF) or exact exchange and a 63% scaling factor for Slater exchange (so the hybrid functional is B3LYP-37)^[11-14]. The same 6-31G(d,p) basis function is used along with B3LYP-37 functional^[15]. Polarizable continuum model (PCM)^[13] with various solvents (same as investigated in experiment) was applied in the TD-DFT^[16-19] formalism to study the solvent effects on the optical absorption and emission properties of the studied dyes. The spin-orbit coupling matrix elements $\langle S_1 | H_{SO} | T_n \rangle$ between the singlet (S_1) state and the energy lower state state T_n were calculated at the TDDFT/B3LYP/6-31G(d,p) level using MOLSOC program.^[20]

The k_{IC} , k_r rate constants and fluorescence quantum yield (ϕ_f) were calculated using the algorithm described in References.^[21-23] This algorithm uses the quantum chemical computed matrix elements, energies such as the nonadiabatic coupling matrix elements (NACME), between the S_1 and S_0 states, the spin-orbit coupling matrix elements (SOCME) between S_1 and energy lower triplet electronic states, and the transition electric dipole moment between the S_1 and S_0 states as the input parameters. These input data were obtained using the DFT and at the TDDFT level for the ground and excited states using the B3LYP functional and the 6-31G** basis set. Because, here, the TD-DFT/B3LYP-37 theory method significantly overestimates energy of S_1 state, we therefore considered experimental S_1 emission data to calculate the internal conversion rate constants for these investigated dyes. Similarly, we used S_1 energies from experiment (as the de-excitation energy from S_1 to S_0) and calculated oscillator strength (f) values from theory to compute the radiative decay rate constants. Most of the quantum chemical calculations were performed with Gaussian 16.^[24]

The nonradiative rate constants for internal conversion (k_{IC}) and the intersystem crossing rate constants were calculated using Plotnikov's formula^[25] within Herzberg-Teller (HT) and anharmonic, the Dushinsky effect approximations using the Morse oscillator model as^[21]

$$k_{nr} = \sum_n \left| V_{i0,fn} \right|^2 \Gamma_{fn} \left[\Delta_{if}^2 + \frac{\Gamma_{fn}^2}{4} \right]^{-1} \quad (E4),$$

where i is the initial electronic state, f is the final electronic state, n is a vibrational level of f state, Γ_{fn} is the relaxation width of the vibrational level $|fn\rangle$, $\Delta_{if} = |E_{i0} - E_{fn}|$ is the energy difference between the initial and final vibrational states, and $V_{i0,fn}$ is the matrix element of a perturbation operator. The perturbation operator is the spin-orbit coupling interaction for ISC transitions and the non-adiabatic coupling interaction for IC processes. Usually Γ_{fn} is about 10^{14} s^{-1} and does not depend strongly on n , and Δ_{if} is about 100 cm^{-1} and we can assume $k_{nr} = \frac{4}{\Gamma_f} \sum_n \left| V_{i0,fn} \right|^2$.^[25]

The k_{IC} was calculated as

$$k_{IC-HT} = \frac{4}{\Gamma_f} \left(D^2 \left(\sum_n \prod_k g_k^2 \right) + \sum_i P_i^2 t_i^2 \left(\sum_n \prod_{k \neq i} g_k^2 \right) + \sum_{i,j \neq l} W_{ij}^2 t_i^2 b_j^2 \left(\sum_n \prod_{\substack{k \neq i \\ k \neq j}} g_k^2 \right) \right). \quad (\text{E5})$$

Here,

$$g_j = \frac{N_0 N_n \Delta^{b_0/2}}{\alpha} I_n \left(\frac{\Delta+1}{2}, \frac{b_n+b_0}{2} - 1, b_n \right), \quad (\text{E6})$$

$$t_j = N_0 N_n \Delta^{b_0/2} \left(0.5 I_n \left(\frac{\Delta+1}{2}, \frac{b_n+b_0}{2}, b_n \right) - 0.5 b_n I_n \left(\frac{\Delta+1}{2}, \frac{b_n+b_0}{2} - 1, b_n \right) + I_{n-1} \left(\frac{\Delta+1}{2}, \frac{b_n+b_0}{2} - 1, b_n + 1 \right) \right), \quad (\text{E7})$$

$$b_j = (K + \ln \frac{2\beta}{\alpha}) g_j - \frac{N_0 N_n \Delta^{b_0/2}}{\alpha^2} \frac{dI_n \left(\frac{\Delta+1}{2}, \frac{b_n+b_0}{2} - 1, b_n \right)}{d \left(\frac{b_n+b_0}{2} - 1 \right)}. \quad (\text{E8})$$

The wave function of Morse oscillator is $\psi_n(R) = N_n \exp(-z/2) z^{b_n/2} L_n^{b_n}(z)$, where

$z = 2\beta \exp(-\alpha[R - R_e])$, $b_n = 2\beta - 2n - 1$, $\beta = \frac{1}{\alpha} \sqrt{2D_e}$. The D_e value is the dissociation energy, α is

an anharmonicity constant, R_e is the equilibrium distance, $N_n = \left(\frac{\alpha b_n n!}{\Gamma(b_n + n + 1)} \right)^{1/2}$, $L_n^{b_n}(z)$ is the n -th

Laguerre polynomial, and $\Gamma(b_n + n + 1)$ is a Gamma function. Parameters De and α can be obtained from the anharmonicity parameter χ and the energy ω as $De = \omega/4\chi$ and $\alpha = \sqrt{2\omega\chi}$. We used 0.02 for χ .

Here, $\Delta = \exp(-\alpha K)$, $I_n(A, B, C) = \int_0^\infty \exp(-Az) z^B L_n^C(z) dz$, K is the displacement of oscillator

equilibrium position. In eq. (E8) $\frac{dI_n \left(\frac{\Delta+1}{2}, \frac{b_n+b_0}{2} - 1, b_n \right)}{d \left(\frac{b_n+b_0}{2} - 1 \right)} = \frac{dI_n(A, B, C)}{d(B)}$ and can be estimated numerically. The $I_n(A, B, C)$ can be written analytically as:

$$I_n(A, B, C) = \frac{\Gamma(1+B)\Gamma(C+n+1)}{\Gamma(n+1)\Gamma(C+1)} A^{-1-B} {}_2F_1(1+B, -n, 1+C, \frac{1}{A}). \quad (\text{E9})$$

The second term in eq (E4) is Franck-Condon (FC) one, the first and the third are Herzberg-Teller terms. The D , \dot{P} and W concern the nonadiabatic coupling matrix elements between the i -th and f -th electronic states and are expressed as

$$W_{jj'} = -\sum_v \sum_q \sum_{v'} \sum_{q'} \left\langle \frac{\varphi_i(\mathbf{r}, \mathbf{s}, \mathbf{R}) \partial^2 \varphi_f(\mathbf{r}, \mathbf{s}, \mathbf{R})}{\partial R_{vq} R_{v'q'}} \right\rangle |_{\mathbf{R}=\mathbf{R}_0} M_v^{-1/2} M_{v'}^{-1/2} L_{vqj} L_{v'q'j'} \quad (\text{E10}),$$

$$D = -\sum_v \sum_q (2M_v)^{-1} \left\langle \varphi_i(\mathbf{r}, \mathbf{s}, \mathbf{R}) \left| \frac{\partial^2}{\partial R_{vq}^2} \right| \varphi_f(\mathbf{r}, \mathbf{s}, \mathbf{R}) \right\rangle |_{\mathbf{R}=\mathbf{R}_0} \quad (\text{E11}),$$

$$P_j = -\sum_v \sum_q M_v^{-1/2} L_{vqj} \left\langle \varphi_i(\mathbf{r}, \mathbf{s}, \mathbf{R}) \frac{\partial \varphi_f(\mathbf{r}, \mathbf{s}, \mathbf{R})}{\partial R_{vq}} \right\rangle |_{\mathbf{R}=\mathbf{R}_0} \quad (\text{E12}).$$

Here, $\left\langle \varphi_i(\mathbf{r}, \mathbf{s}, \mathbf{R}) \frac{\partial \varphi_f(\mathbf{r}, \mathbf{s}, \mathbf{R})}{\partial R_{vq}} \right\rangle |_{\mathbf{R}=\mathbf{R}_0}$ and $\left\langle \frac{\varphi_i(\mathbf{r}, \mathbf{s}, \mathbf{R}) \partial^2 \varphi_f(\mathbf{r}, \mathbf{s}, \mathbf{R})}{\partial R_{vq} R_{v'q'}} \right\rangle |_{\mathbf{R}=\mathbf{R}_0}$ are the nonadiabatic

coupling matrix elements (NACMEs) of the first and second order, respectively. M_v is the mass of the v^{th} atom, L_{vqj} are coefficients of the linear relation between the Cartesian (R) and the normal coordinates (Q):

$$R_{vq} - R_{0vq} = M_v^{-1/2} L_{vqj} Q_j.$$

The Lagrange multipliers technique applies to $\prod_{\substack{k \neq i \\ k \neq j}} g_k^2$ at HT-approximation and to $\prod_{k \neq i} g_k^2$ at FC

approximation. The Lagrange function is $L = \ln \left[\prod_{k=1}^{3N-6} \left(\frac{e^{-y_k} y_k^{n_k}}{n_k!} \right) \right] - \lambda \left(\sum_{k=1}^{3N-6} n_k \omega_k + E_{if} \right)$, and the solution of

$$\left(\sum_{k=1}^{3N-6} y_k \exp(-\omega_k \lambda) \omega_k \right) = E_{if} \text{ leads to } n_k = y_k \exp(-\omega_k \lambda), \text{ where } \lambda \text{ is the Lagrange multiplier. The}$$

Dushinsky effect was included in W and P matrix and vector as^[21]

$$\tilde{P}_i = \sum_l P_l J_{li} + \sum_{l,m \neq l} K_l P_{lm} J_{mi}, \quad (\text{E13})$$

$$\tilde{W}_{ij} = \sum_{l,m \neq l} P_{lm} J_{li} J_{mj}. \quad (\text{E14})$$

Here J is Dushinsky matrix.

The radiative rate constants (k_r) are calculated as^[26]

$$k_r(p \rightarrow q) = \frac{1}{1.5} f \cdot E_{pq}, \quad (\text{E15})$$

where f is the oscillator strength.

The nonradiative rate constants for intersystem crossing k_{ISC} are calculated as^[26]

$$k_{ISC} = \frac{4}{\Gamma_f} \sum_{n_1, n_2, \dots, n_{3N-6}}^{E_{if} = n_1\omega_1 + n_2\omega_2 + \dots + n_{3N-6}\omega_{3N-6}} \left(H_{SO}^{if} \Big|_{R=R_0}^r \left[\prod_{k=1}^{3N-6} \left(\frac{e^{-y_k} y_k^{n_k}}{n_k!} \right)^{1/2} \right] + \sum_{j=1}^{3N-6} t_j W_j \cdot \left[\prod_{\substack{k=1 \\ k \neq j}}^{3N-6} \left(\frac{e^{-y_k} y_k^{n_k}}{n_k!} \right)^{1/2} \right] \right)^2 \quad (\text{E16})$$

where the W_j is given by $W_j = \sum_v \sum_q \frac{\partial H_{SO}^{if}}{\partial R_{vq}} \Big|_{R=R_0}^r M_v^{-1/2} L_{vqj}$. Here H_{SO}^{if} is matrix element of SOC-operator.

The fluorescence quantum yield from the S_I state can be obtained as^[27]

$$\varphi_{fl} = \frac{k_r}{k_r + k_{IC} + \sum_i k_{IST_i}}, \quad (\text{E17})$$

where k_{IST_i} is a ISC rate constant between S_I and energetically lower triplet states T_i , k_r and k_{IC} are radiative and IC rate constants of the electronic transition from S_I to the ground state S_0 , respectively.

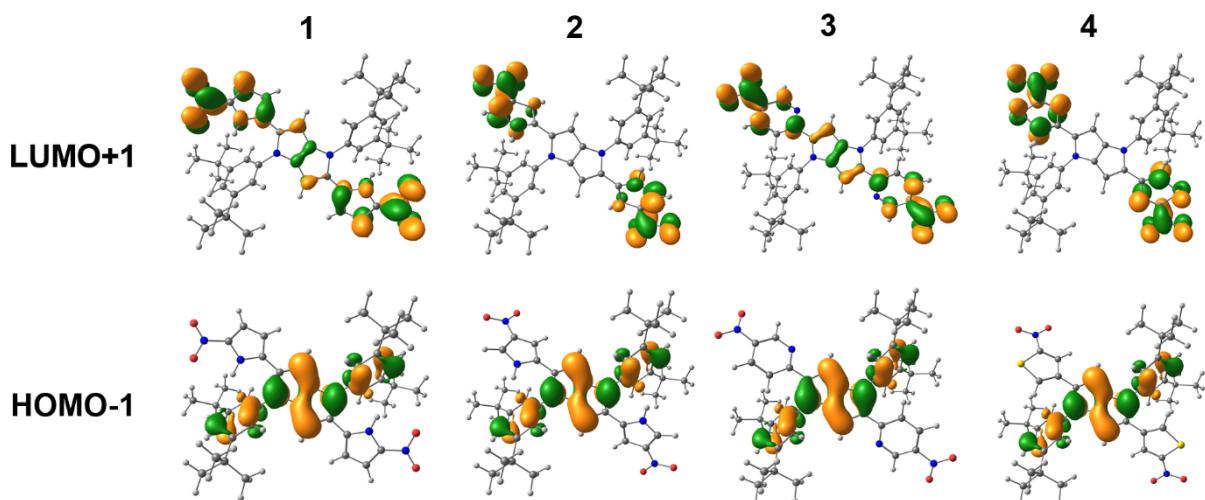


Fig. S17. Representation of charge density distribution in HOMO-1 and LUMO+1 orbitals of the studied dyes. Computed LUMO (shown in MS) and LUMO+1 orbitals of dyes **2** and **4** are nearly degenerate.

Table S1: Calculated TD-DFT/B3LYP-37/6-31G(d,p) theory level optical absorption for dye **1**.

Solvents	Transitions	Wavelength (nm)	Energy (eV)	Osc. strength
n-haxane	S0→S1	461	2.69	1.4964
	S0→S2	386	3.21	0.0138
	S0→S3	351	3.53	0.0772
	S0→S4	311	3.98	0.0021
	S0→S5	303	4.09	0.0012
Toluene	S0→S1	468	2.65	1.5387
	S0→S2	389	3.18	0.0144
	S0→S3	354	3.50	0.0767
	S0→S4	314	3.95	0.0020
	S0→S5	302	4.11	0.0018
PE	S0→S1	473	2.62	1.5180
	S0→S2	396	3.13	0.0153
	S0→S3	362	3.42	0.0666
	S0→S4	321	3.86	0.0016
	S0→S5	303	4.09	0.0144
THF	S0→S1	473	2.62	1.5063
	S0→S2	395	3.14	0.0137
	S0→S3	363	3.41	0.0640
	S0→S4	322	3.84	0.0014
	S0→S5	303	4.09	0.0135
EtAc	S0→S1	471	2.63	1.4937
	S0→S2	394	3.15	0.0135
	S0→S3	362	3.42	0.0645
	S0→S4	321	3.86	0.0014
	S0→S5	302	4.10	0.0127
n-octanol	S0→S1	475	2.61	1.5153
	S0→S2	397	3.13	0.0138
	S0→S3	365	3.40	0.0630
	S0→S4	324	3.83	0.0013
	S0→S5	303	4.08	0.0140
BuAc	S0→S1	470	2.64	1.5021
	S0→S2	393	3.15	0.0137
	S0→S3	361	3.44	0.0660
	S0→S4	320	3.87	0.0015
	S0→S5	302	4.11	0.0118
CH3CN	S0→S1	475	2.61	1.4841
	S0→S2	398	3.12	0.0133
	S0→S3	368	3.37	0.0582
	S0→S4	327	3.80	0.0012
	S0→S5	304	4.07	0.0146

Table S2: Calculated TD-DFT/B3LYP-37/6-31G(d,p) theory level optical S1→S0 emission for dye **1**.

Solvents	Wavelength (nm)	Energy (eV)	Osc. strength
n-haxane	504	2.46	1.7780
Toluene	513	2.42	1.8304
PB	553	2.24	2.0389
THF	562	2.21	2.0846
EtAc	555	2.23	2.0523
n-octanol	570	2.17	2.1196
Bu Ac	549	2.26	2.0212
CH3CN	590	2.10	2.2071

Table S3: Calculated TD-DFT/B3LYP-37/6-31G(d,p) theory level optical absorption for dye **2**.

Solvents	Transitions	Wavelength (nm)	Energy (eV)	Osc. strength
Toluene	S0→S1	385	3.22	0.2035
	S0→S2	382	3.25	0.0099
	S0→S3	326	3.80	1.1371
	S0→S4	300	4.14	0.0667
	S0→S5	299	4.15	0.0000
PE	S0→S1	398	3.12	0.1903
	S0→S2	393	3.15	0.0090
	S0→S3	324	3.83	1.1356
	S0→S4	309	4.01	0.0566
	S0→S5	307	4.04	0.0011
THF	S0→S1	400	3.10	0.1933
	S0→S2	396	3.13	0.0091
	S0→S3	324	3.83	1.1460
	S0→S4	311	3.99	0.0557
	S0→S5	309	4.01	0.0011
EtAc	S0→S1	398	3.11	0.1893
	S0→S2	394	3.14	0.0090
	S0→S3	323	3.83	1.1335
	S0→S4	310	4.01	0.0558
	S0→S5	307	4.03	0.0011
n-octanol	S0→S1	403	3.08	0.1966
	S0→S2	398	3.11	0.0092
	S0→S3	324	3.83	1.1556
	S0→S4	313	3.97	0.0555
	S0→S5	310	3.99	0.0011
Bu Ac	S0→S1	396	3.13	0.1911
	S0→S2	392	3.16	0.0091
	S0→S3	324	3.83	1.1366
	S0→S4	308	4.02	0.0576
	S0→S5	306	4.05	0.0011
CH3CN	S0→S1	407	3.04	0.1914
	S0→S2	403	3.08	0.0087
	S0→S3	322	3.85	1.1342
	S0→S4	316	3.92	0.0552
	S0→S5	314	3.95	0.0010
MeOH	S0→S1	407	3.05	0.1896
	S0→S2	402	3.08	0.0086
	S0→S3	322	3.85	1.1290
	S0→S4	316	3.92	0.0551
	S0→S5	314	3.95	0.0010

Table S4: Calculated TD-DFT/B3LYP-37/6-31G(d,p) theory level optical S1→S0 emission for dye **2**.

Solvents	Wavelength (nm)	Energy (eV)	Osc. strength
Toluene	570	2.17	0.0731
PB	602	2.06	0.1031
THF	609	2.03	0.1119
EtAc	604	2.05	0.1059
n-octanol	615	2.01	0.1190
Bu Ac	599	2.07	0.0999
CH3CN	629	1.97	0.1378
MeOH	628	1.97	0.1370

Table S5: Calculated TD-DFT/B3LYP-37/6-31G(d,p) theory level optical absorption for dye **3**.

Solvents	Transitions	Wavelength (nm)	Energy (eV)	Osc. strength
n-hexane	S0→S1	468	2.65	1.5619
	S0→S2	393	3.15	0.0980
	S0→S3	380	3.26	0.0035
	S0→S4	336	3.69	0.0006
	S0→S5	308	4.02	0.0001
Toluene	S0→S1	474	2.61	1.6020
	S0→S2	396	3.13	0.1000
	S0→S3	384	3.23	0.0035
	S0→S4	339	3.66	0.0006
	S0→S5	307	4.03	0.0002
CH3CN	S0→S1	477	2.60	1.5364
	S0→S2	405	3.06	0.0938
	S0→S3	390	3.18	0.0035
	S0→S4	348	3.56	0.0007
	S0→S5	313	3.96	0.0023
THF	S0→S1	477	2.60	1.5632
	S0→S2	403	3.08	0.0960
	S0→S3	389	3.19	0.0035
	S0→S4	346	3.59	0.0007
	S0→S5	311	3.99	0.0023
EtAc	S0→S1	475	2.61	1.5516
	S0→S2	402	3.08	0.0957
	S0→S3	387	3.20	0.0035
	S0→S4	345	3.59	0.0006
	S0→S5	310	3.99	0.0022
PE	S0→S1	475	2.61	1.5566
	S0→S2	402	3.09	0.0960
	S0→S3	387	3.20	0.0035
	S0→S4	344	3.60	0.0006
	S0→S5	310	4.00	0.0022
n-octanol	S0→S1	478	2.59	1.5712
	S0→S2	403	3.07	0.0961
	S0→S3	390	3.18	0.0035
	S0→S4	347	3.58	0.0007
	S0→S5	312	4.00	0.0023
BuAc	S0→S1	475	2.61	1.5609
	S0→S2	401	3.09	0.0963
	S0→S3	387	3.20	0.0035
	S0→S4	344	3.60	0.0006
	S0→S5	310	4.00	0.0022

Table S6: Calculated TD-DFT/B3LYP-37/6-31G(d,p) theory level optical S1→S0 emission for dye **3**.

Solvents	Wavelength (nm)	Energy (eV)	Osc. strength
n-hexane	516	2.40	1.6754
Toluene	528	2.35	1.7455
CH3CN	597	2.08	2.0950
THF	572	2.17	1.9793
EtAc	566	2.19	1.9482
PE	563	2.20	1.9345
n-octanol	579	2.14	2.0129
Bu Ac	560	2.21	1.9173

Table S7: Calculated TD-DFT/B3LYP-37/6-31G(d,p) theory level optical absorption for dye 4.

Solvents	Transitions	Wavelength (nm)	Energy (eV)	Osc. strength
n-hexane	S0→S1	473	2.62	0.0358
	S0→S2	472	2.63	0.0067
	S0→S3	371	3.34	0.0137
	S0→S4	368	3.36	0.0009
	S0→S5	333	3.72	1.3750
Toluene	S0→S1	478	2.59	0.0361
	S0→S2	477	2.60	0.0071
	S0→S3	374	3.31	0.0159
	S0→S4	372	3.33	0.0010
	S0→S5	335	3.70	1.4280
PE	S0→S1	489	2.54	0.0302
	S0→S2	488	2.54	0.0066
	S0→S3	382	3.25	0.0166
	S0→S4	380	3.26	0.0009
	S0→S5	334	3.72	1.4114
THF	S0→S1	491	2.52	0.0299
	S0→S2	490	2.53	0.0066
	S0→S3	383	2.23	0.0173
	S0→S4	381	3.25	0.0009
	S0→S5	334	3.71	1.4247
EtAc	S0→S1	489	2.53	0.0298
	S0→S2	489	2.54	0.0065
	S0→S3	382	3.24	0.0166
	S0→S4	380	3.26	0.0009
	S0→S5	333	3.72	1.4082
n-octanol	S0→S1	493	2.52	0.0299
	S0→S2	492	2.52	0.0067
	S0→S3	384	3.22	0.0179
	S0→S4	383	3.24	0.0009
	S0→S5	334	3.71	1.4379
Bu Ac	S0→S1	488	2.54	0.0307
	S0→S2	487	2.55	0.0066
	S0→S3	381	3.25	0.0166
	S0→S4	379	3.27	0.0009
	S0→S5	334	3.71	1.4133
CH3CN	S0→S1	496	2.50	0.0277
	S0→S2	496	2.50	0.0064
	S0→S3	387	3.20	0.0176
	S0→S4	385	3.22	0.0009
	S0→S5	333	3.72	1.4132

Table S8: Calculated TD-DFT/B3LYP-37/6-31G(d,p) theory level optical S1→S0 emission for dye 4.

Solvents	Wavelength (nm)	Energy (eV)	Osc. strength
n-hexane	664	1.87	0.0094
Toluene	678	1.83	0.0103
PB	716	1.73	0.0129
THF	725	1.71	0.0136
EtAc	719	1.73	0.0131
n-octanol	732	1.69	0.0142
Bu Ac	712	1.74	0.0126
CH3CN	750	1.65	0.0159

4. References

- [1] J. Hrabovský, J. Kováč and K. Vagáčová, Collect. Czechoslov. Chem. Commun., **1986**, 51, 1301–1303.
- [2] M. Tasior, O. Vakuliuk, D. Koga, B. Koszarna, K. Górska, M. Grzybowski, Ł. Kielesiński, M. Krzeszewski and D. T. Gryko, J. Org. Chem., **2020**, 85, 13529–13543.
- [3] M. Sheik-Bahae, A. A. Said, T. H. Wei, D. J. Hagan, E. W. van Stryland, IEEE J. Quantum Electron. **1990**, 26, 760.
- [4] K. Kamada, K. Matsunaga, A. Yoshino, K. Ohta, J. Opt. Soc. Am. B **2003**, 20, 529.
- [5] K. Kamada, Y. Iwase, K. Sakai, K. Kondo, K. Ohta, J. Phys. Chem. C **2009**, 113, 11469.
- [6] K. Kamada, C. Hara, K. Ogawa, K. Ohta, Y. Kobuke, Chem. Comm. **2012**, 48, 7988.
- [7] S. Hirata, M. Head-Gordon, Chem. Phys. Lett. **1999**, 314, 291.
- [8] Gaussian 16, Revision C.01, M. J. Frisch, G. W. Trucks, H. B. Schlegel, G. E. Scuseria, M. A. Robb, J. R. Cheeseman, G. Scalmani, V. Barone, G. A. Petersson, H. Nakatsuji, X. Li, M. Caricato, A. V. Marenich, J. Bloino, B. G. Janesko, R. Gomperts, B. Mennucci, H. P. Hratchian, J. V. Ortiz, A. F. Izmaylov, J. L. Sonnenberg, D. Williams-Young, F. Ding, F. Lipparini, F. Egidi, J. Goings, B. Peng, A. Petrone, T. Henderson, D. Ranasinghe, V. G. Zakrzewski, J. Gao, N. Rega, G. Zheng, W. Liang, M. Hada, M. Ehara, K. Toyota, R. Fukuda, J. Hasegawa, M. Ishida, T. Nakajima, Y. Honda, O. Kitao, H. Nakai, T. Vreven, K. Throssell, J. A. Montgomery, Jr., J. E. Peralta, F. Ogliaro, M. J. Bearpark, J. J. Heyd, E. N. Brothers, K. N. Kudin, V. N. Staroverov, T. A. Keith, R. Kobayashi, J. Normand, K. Raghavachari, A. P. Rendell, J. C. Burant, S. S. Iyengar, J. Tomasi, M. Cossi, J. M. Millam, M. Klene, C. Adamo, R. Cammi, J. W. Ochterski, R. L. Martin, K. Morokuma, O. Farkas, J. B. Foresman, and D. J. Fox, Gaussian, Inc., Wallingford CT, **2019**.
- [9] J. B. Foresman, A. Frisch, “Exploring Chemistry with Electronic Structure Methods”, 2nd Ed. (**1993**) Gaussian Inc., Pittsburgh.
- [10] K. Ohta, S. Yamada, K. Kamada, A. D. Slepkov, F. A. Hegmann, R. R. Tykwinski, L. D. Shirtcliff, M. M. Haley, P. Sałek, F. Gel'mukhanov, H. Ågren, J. Phys. Chem. A **2011**, 115, 105.
- [11] A. D. Becke, J. Chem. Phys., **1993**, 98, 5648-5652.
- [12] C. Lee, W. Yang and R. G. Parr, Physical Review B, **1988**, 37, 785-789.
- [13] R. Ditchfield, W. J. Hehre and J. A. Pople, J. Chem. Phys., **1971**, 54, 724-728.
- [14] M. J. Frisch, J. A. Pople and J. S. Binkley, J. Chem. Phys., **1984**, 80, 3265-3269.
- [15] J. Tomasi, B. Mennucci and R. Cammi, Chem. Rev., **2005**, 105, 2999-3094.
- [16] R. Bauernschmitt and R. Ahlrichs, Chem. Phys. Lett., **1996**, 256, 454-464.
- [17] M. E. Casida, C. Jamorski, K. C. Casida and D. R. Salahub, J. Chem. Phys., **1998**, 108, 4439-4449.
- [18] R. E. Stratmann, G. E. Scuseria and M. J. Frisch, J. Chem. Phys., **1998**, 109, 8218-8224.
- [19] G. Scalmani, M. J. Frisch, B. Mennucci, J. Tomasi, R. Cammi and V. Barone, J. Chem. Phys., **2006**, 124, 094107: 1-15.
- [20] S. G. Chiodo, M. Leopoldini, MolSOC: A spin-orbit coupling code. Computer Physics Communications **2014**, 185 (2), 676-683.
- [21] R. R. Valiev, B. S. Merzlikin, R. T. Nasibullin, A. Kurtzevitch, V. N. Cherepanov, R. R. Ramazanov, D. Sundholm and T. Kurten, Phys. Chem. Chem. Phys., **2023**, 25, 6406–6415.
- [22] R. R. Valiev, R. T. Nasibullin, V. N. Cherepanov, A. Kurtsevich, D. Sundholm and T. Kurtén, Phys. Chem. Chem. Phys., **2021**, 23, 6344-6348.
- [23] R. R. Valiev, R. T. Nasibullin, V. N. Cherepanov, G. V. Baryshnikov, D. Sundholm, H. Ågren, B. F. Minaev and T. Kurtén, Phys. Chem. Chem. Phys., **2020**, 22, 22314-22323.
- [24] Gaussian 16, Revision B.01, M. J. Frisch, G. W. Trucks, H. B. Schlegel, G. E. Scuseria, M. A. Robb, J. R. Cheeseman, G. Scalmani, V. Barone, G. A. Petersson, H. Nakatsuji, X. Li, M. Caricato, A. V. Marenich, J. Bloino, B. G. Janesko, R. Gomperts, B. Mennucci, H. P. Hratchian, J. V. Ortiz, A. F. Izmaylov, J. L. Sonnenberg, D. Williams-Young, F. Ding, F. Lipparini, F. Egidi, J. Goings, B. Peng, A. Petrone, T. Henderson, D. Ranasinghe,

V. G. Zakrzewski, J. Gao, N. Rega, G. Zheng, W. Liang, M. Hada, M. Ehara, K. Toyota, R. Fukuda, J. Hasegawa, M. Ishida, T. Nakajima, Y. Honda, O. Kitao, H. Nakai, T. Vreven, K. Throssell, J. A. Montgomery, Jr., J. E. Peralta, F. Ogliaro, M. J. Bearpark, J. J. Heyd, E. N. Brothers, K. N. Kudin, V. N. Staroverov, T. A. Keith, R. Kobayashi, J. Normand, K. Raghavachari, A. P. Rendell, J. C. Burant, S. S. Iyengar, J. Tomasi, M. Cossi, J. M. Millam, M. Klene, C. Adamo, R. Cammi, J. W. Ochterski, R. L. Martin, K. Morokuma, O. Farkas, J. B. Foresman and D. J. Fox, Gaussian, Inc., Wallingford CT, **2016**.

[25] V. G. Plotnikov, *Int J Quantum Chem.*, **1979**, *16* (3), 527–541.

[26] R. R. Valiev, V. N. Cherepanov, R. T. Nasibullin, D. Sundholm, and T. Kurten, *Phys. Chem. Chem. Phys.* **2019**, *21* (34), 18495–18500.

[27] E. S. Medvedev and V. I. Osherov, **1995**, *57*, doi:10.1007/978-3-642-85109-4.